HHS Public Access

Author manuscript

*J Mol Cell Cardiol*. Author manuscript; available in PMC 2016 July 01.

Published in final edited form as:

*J Mol Cell Cardiol*. 2015 July ; 84: 70–80. doi:10.1016/j.yjmcc.2015.04.007.

# Lumican Deficiency Results In Cardiomyocyte Hypertrophy With Altered Collagen Assembly

**Loren E. Dupuis**[1], **Matthew G. Berger**[2], **Samuel Feldman**[2], **Lorna Doucette**[2], **Vennece Fowlkes**[1], **Shukti Chakravarti**[3], **Sarah Thibaudeau**[1], **Nicolas E. Alcala**[2], **Amy D. Bradshaw**[4], and **Christine B. Kern**[1]

[1]Department of Regenerative Medicine and Cell Biology, Medical University of South Carolina, Charleston, SC 29425

[2]Honors College, College of Charleston, Charleston, SC, 29401

[3]Department of Medicine, Johns Hopkins School of Medicine, Baltimore, MD 21205

[4]Gazes Cardiac Research Institute, Medical University of South Carolina, Charleston, SC 29425

## Abstract

The ability of the heart to adapt to increased stress is dependent on modification of its extracellular matrix (ECM) architecture that is established during postnatal development as cardiomyocytes differentiate, a process that is poorly understood. We hypothesized that the small leucine-rich proteoglycan (SLRP) lumican (LUM), which binds collagen and facilitates collagen assembly in other tissues, may play a critical role in establishing the postnatal murine myocardial ECM. Although previous studies suggest LUM deficient mice (*lum*$^{-/-}$) exhibit skin anomalies consistent with Ehlers-Danlos syndrome, *lum*$^{-/-}$ hearts have not been evaluated. These studies show LUM was immunolocalized to non-cardiomyocytes of the cardiac ventricles and its expression increased throughout development. Lumican deficiency resulted in significant (50%) perinatal death and further examination of the *lum*$^{-/-}$ neonatal hearts revealed an increase in myocardial tissue without a significant increase in cell proliferation. However cardiomyocytes from surviving postnatal day 0 (P0), 1 month (1 mo) and adult (4 mo) *lum*$^{-/-}$ hearts were significantly larger than their wild type (WT) littermates. Immunohistochemistry revealed that the increased cardiomyocyte size in the *lum*$^{-/-}$ hearts correlated with alteration of the cardiomyocyte pericellular ECM components collagenα1(I) and the class I SLRP decorin (DCN). Western blot analysis demonstrated that the ratio of glycosaminoglycan (GAG) decorated DCN to core DCN was reduced in P0 and 1 mo *lum*$^{-/-}$ hearts. There was also a reduction in the β and γ forms of collagenα1(I) in *lum*$^{-/-}$ hearts. While the total insoluble collagen content was significantly reduced, the fibril size was increased in *lum*$^{-/-}$ hearts, indicating LUM may play a role in collagen fiber stability and lateral fibril assembly. These results suggest that LUM controls cardiomyocyte growth by regulating the



**Disclosures:** None of the Authors have any disclosures to report.

pericellular ECM and also indicates that LUM may coordinate multiple factors of collagen assembly in the murine heart. Further investigation into the role of LUM may yield novel therapeutic targets and/or biomarkers for patients with cardiovascular disease.

**Keywords**

lumican; decorin; collagen; fibroblast; hypertrophy; SLRP; myocardium; cardiomyocyte; ECM; proteoglycan

## 1. Introduction

Cardiac hypertrophy is generally defined as a reactive increase in cardiac size and myocardial mass in response to hemodynamic stress[1, 2]. In pathophysiological conditions, cardiomyocytes enlarge and it's the enlargement of these contractile cells of the heart that results in an increase in organ size referred to as cardiac hypertrophy. However cardiomyocytes also expand in size during postnatal development where they switch from a stellate appearance to their characteristic rod-shaped mature phenotype. In an effort not to confuse the developmental cardiomyocyte cell enlargement after birth with pathological cell enlargement referred to as 'hypertrophy' we refer to the normal postnatal cardiac growth as eutrophy which, remains a relatively understudied developmental process by which cardiomyocytes enlarge as they mature which in turn causes the heart to expand, without significant cell proliferation [1].

In recent years there has been considerable investigation into defining the molecular markers involved in the specification of the cardiomyocyte progenitors. In addition, the examination of cell lineages, largely through CRE-lineage tracing, has established multiple origins of cardiomyocytes that comprise the fully formed mammalian heart. Significantly less is known about the maturation of cardiomyocytes from fetal stages onward [3]. Importantly, after birth cardiomyocytes switch from proliferative to eutrophic growth [4]. This transition from proliferative progenitors to differentiated cardiomyocytes requires exquisite timing to down-regulate developmental pathways and to upregulate terminal differentiation gene programs. Several pathways that promote proliferation actively work to prevent differentiation therefore maintaining the balance of pathways is important for normal cardiomyocyte differentiation and eutrophic growth[3].

Coincident with cardiomyocyte differentiation is the maturation of the extracellular matrix (ECM) architecture within the ventricles of the postnatal heart. In fact, the ECM structure is responsible for the rod-shaped phenotype of the adult cardiomyocytes [5, 6]. Although ECM maturation often mirrors cardiovascular cell differentiation, the interconnection between ECM architecture and cell signaling programs that balance growth and differentiation remain poorly understood. There is mounting evidence that both the provisional and mature ECM is generated by the cardiac fibroblasts. Since collagen is required to maintain the integrity and biomechanical properties of the mature four-chambered heart [7–9] one of the major roles of the embryonic and adult cardiac fibroblasts is the adequate assembly of collagen fibers. In the ventricular myocardium the organization of the mature collagen network is established within the first months of postnatal life and maintained in the adult.

Although the collagens comprise a major part of the cardiac ECM it is becoming increasingly evident that not all patients with collagen-related disorders have mutations in collagen genes or genes encoding enzymes that directly modify collagen. Therefore other classes of molecules that are integral for correct collagen assembly may also play a role in establishing and maintaining the cardiovascular ECM. The small leucine rich proteoglycans (SLRPs) are a class of ECM molecules that contain leucine rich repeats (LRR) and bind directly to collagen fibers to modify collagen assembly and growth[10–13]. We speculate that postnatal cardiac development is an important period to investigate the role of SLRPs and other factors responsible for the assembly of the collagen-rich matrix that is coincident with cardiomyocyte differentiation and eutrophy.

In this study we examined for the first time, the role of the class II SLRP lumican (LUM) in the developing murine heart. Previous studies using mouse models of LUM deficiency have determined its requirement for normal collagen fiber assembly in the skeletal muscle, [14] tendon [15] and cornea [16, 17]. We evaluated the spatiotemporal localization of LUM throughout cardiac development and using a LUM deficient mouse model determine a potentially critical role for LUM in murine cardiac development.

## 2. Materials and Methods

### 2.1 Mice

All mouse experiments were done under protocols approved by the Medical University of South Carolina IACUC. The lumican deficient mice (*lum*$^{-/-}$) used in this study were received from S. Chakravarti [18] and were bred into C57BL/6 (> 10 generations).

### 2.2 Histology and Immunohistochemistry

Standard histological procedures were used [19]. The lumican antibodies used included a gift from Dr. A. Oldberg, Lund University and a lumican anibody against mouse from R & D Systems™ (AF2846); Laminin antibody was purchased from Abcam (ab11575). Collagenα1(I) was purchased from mdbioproducts (203002) and Decorin was obtained from R & D systems™ (RF1060). Antibodies to α sarcormeric actin (Sigma, A2172), and α smooth muscle actin (Sigma, A 5228) were also utilized in this study to identify myocardial and smooth muscle cells respectively. Fluor-conjugated secondary antibodies were purchased from Jackson ImmunoResearch (West Grove, PA). Antibodies were used in murine tissues fixed in Amsterdam [20] and 4% paraformaldehyde as well as cryopreserved sections. All 4% paraformaldehyde tissue was also paired with citric acid antigen unmasking (H-3300, Vector laboratories, Burlingame CA). Imaging was performed on the Leica TCS SP5 AOBS Confocal Microscope System (Leica Microsystems Inc., Exton, PA).

### 2.3 Myocardial area and heart size measurements

Histological sections (four sections/heart) from wild type (n=8) and *lum*$^{-/-}$ (n=8) P0 mice, over a 20μm depth concomitant with the aortic valve, were used to determine muscle area in Amira™. The average ventricular area was measured in positive pixels in wild type and *lum*$^{-/-}$ littermates from two different litters. A set rectangular area was placed over the

widest part of the right ventricle, septum and left ventricle and used for area measurements. Four sections were used per heart for pixel area.

The heart size was analyzed in wild type and *lum*$^{-/-}$ littermates at P0 and 1 month. The width and length of the hearts were quantified using the Olympus BX40 light microscope and accompanying software. Student's t-test, followed by Anova was utilized to determine statistical significance. P0 hearts; WT (n=8), *lum*$^{-/-}$ (n=8). 1 month; WT (n=10), *lum*$^{-/-}$ (n=8).

### 2.4 Amira™ three-dimensional reconstructions

Using approximately 250, 5 μm thick frontal sections, from each heart were stained with hematoxylin and eosin and used for three-dimensional (3D) reconstructions (n=2 WT; n=3 *lum*$^{-/-}$) at postnatal (P0). All of the heart sections that encompassed the ventricular lumens of the LV and RV from the wt and *lum*−/− were used. The positive pixels that represent cardiac tissue are identified using transparent purple and negative pixels on the internal area of the muscle were denoted in cyan and designate RV and LV lumen space.

### 2.5 Myocardial cell size measurement

The width of cardiomyocytes, defined as nucleated α-sarcomeric actin positive cells, was measured using the ruler tool in Photoshop™. Cardiomyocyte cell borders were delineated using IHC of the basement membrane component laminin. To control for differences in cardiomyocyte cell size within different regions of the murine heart, measurements were taken at the depth of the aortic valve. Cross sections of cardiomyocytes were also grouped and analyzed according to their location within the working myocardium i.e. right ventricle, septum or left ventricle. A total of n ≥ 4 was used for each genotype (WT/ *lum*$^{-/-}$) and represented three aged-matched litters for each time point P0, 1 month (that exhibited increased myocardial area) and n=3 each for adult (4 month-old) WT and *lum*−/−. Student's t-test, followed by Anova was utilized to determine statistical significance.

### 2.6 Electron Microscopy

Sections of hearts preserved in Karnovsky's fixative were generated from 3 wt and 5 *lum*$^{-/-}$ mice at 1 month of age and processed for transmission EM. Collagen fibril diameters were measured in scanned images generated from electron micrographs with NIH image software. Collagen fibrils in at least 3 fields derived from sections of hearts from each mouse were quantified. EM images were taken at ×20,000 magnification were scanned into Adobe Photoshop (Fremont, WA) on an Epson flat bed scanner. A minimum contribution of 200 fibrils from each mouse was counted. Measurement of fibril diameter was performed with the NIH image software program, and data were transferred to the Microsoft Excel program (Redmond, WA) to generate average lengths and distributions of diameters.

### 2.7 Hydoxyproline analysis

Total, insoluble myocardial collagen was quantified using hydroxyproline analysis, as previously described [21]. Briefly, frozen hearts were lyophilized, weighed (dry weight), pulverized, resuspended in 1 M NaCl with protease inhibitors, tumbled overnight at 4°C, and centrifuged. Collagen was quantified as micrograms hydroxyproline per mg dry weight.

Hearts from adult *lum*$^{-/-}$ (*n* = 9), and WT (*n* = 9), were analyzed in this study and following IACUC protocols.

### 2.8 Western blots and quantification

Heart extracts from WT and *lum*$^{-/-}$ deficient mice were prepared using standard RIPA buffer extraction. For collagenα1(I) western blots, 3–8% reducing gradient gels were used. Blots were probed with ColIα1 antibody (mdbioproducts #203002). The DCN blots were from 4–12% reducing gradient gels using the anti-mouse DCN antibody AF1060 from R & D Sytems®. For LUM western blots, 4–12% reducing gels were used. Bands were quantified using ImageJ software. In some cases where the lanes of WT were a dark smear in order to keep the quantification within the linear range we utilized the lanes with less protein loaded (i.e 25 or 12.5μg). Note that the lane background was subtracted in all ImageJ calculations of bands and the internal loading standard of GAPDH expression and protein concentration were included to determine relative density of bands in comparisons of WT versus KO samples. Students t-test, followed by Anova was utilized to determine statistical significance.

## 3. Results

### 3.1 Lumican is expressed within the ventricular myocardium during fetal development and expression is maintained during postnatal stages and in the adult murine heart

LUM was expressed in the developing ventricles of the murine heart; at E15.5 LUM expression was most prevalent within the myocardium surrounding the aortic valve cusp (Fig. 1A, arrowhead) and within the myocardium adjacent to and within the developing trabeculae (Fig. 1A, box). Higher magnification of LUM immunohistochemistry (IHC) showed its expression in noncardiomyocytes (α-sarcomeric actin (α-sarc) negative) of the left ventricle (LV) (Fig. 1B, arrow). The E15.5 ventricular pattern of expression was maintained in the E17.5 hearts (Fig. 1C). Shortly after birth (P0) LUM was prevalent adjacent to α-sarc positive, stellate shaped-cardiomyocytes (Fig. 1D, arrow). At P0 LUM expression was greater in the noncompacted myocardium compared to the highly compacted myocardium of the outer walls; LUM expression in the septum was similar to that observed in the LV trabeculae (Fig. 1C) data not shown. In one-month (1 mo) hearts the most intense lumican IHC was subjacent to the ventricular lumen and in the outer layers of compact myocardium of the ventricular wall (Fig. 1E, box). High magnification of these regions demonstrated that lumican was expressed subjacent to cardiomyocytes (Fig. 1F, arrow) but not detected in myocardial (α-sarc positive) cells. LUM was also expressed within the adult (>4 mo) murine heart and appeared as punctate staining on cardiomyocytes and other α-sarc negative cells (Fig. 1G, H, arrow). The expression of LUM in the adult was similar to that at 1 mo with a highest level of detection in myocardium near the lumen (Fig. 1G, H). Of note, the detection of LUM via immunolocalization was significantly more difficult to optimize in histological sections from adult hearts compared to 1 mo heart sections in all fixatives and unmasking techniques utilized. The 4% paraformaldehyde fixative gave the most consistent results for LUM IHC at 4 mo, albeit the intensity of IHC staining was reduced compared to 1 mo (Fig. 1G, H). The difficulty in detecting LUM by IHC may be due to the fact that the

epitopes are masked in the more mature collagen fibers of the adult murine heart since there is more LUM protein in adult hearts than other younger stages.

Although other studies had determined that there was a relative increase in lumican mRNA during heart development [22], *lum* protein expression had not been assessed. Using protein extracts from hearts at P0, 1 mo and adult (4 mo) we examined the expression of LUM in postnatal hearts; lysates from $lum^{-/-}$ P0, 1 mo and 4 mo hearts were also utilized to denote lumican-specific bands. In P0 heart lysates there were two bands with a MW of 50 and 60 respectively (Fig. 1I, open arrows). In later stage heart extracts from 1 mo and 4 mo the intense bands had shifted upward with a band that was barely visible at 50 kD (Fig. 1I, open arrows) in longer exposures. Shorter exposure (Fig. 1I*) revealed that the upper bands in $lum^{+/+}$ 1 mo and 4 mo extracts resolved into three distinct bands between 60-75 kD from 1 mo and 4 mo lysates however the lower two bands of this triplicate were slightly higher MWs at 4 mo (Fig. 1I, solid arrows*). The increase in MW of LUM during postnatal development would be consistent with elongation of the keratan sulfate glycosaminoglycan modification of LUM in aging hearts. Moreover the prominent mature forms ranging from 65–75 kD were absent at P0 (Fig. 1I, open arrowheads). Of note lysates from $lum^{-/-}$ P0, 1 mo and 4 mo hearts revealed absence of these bands. In long exposures there was a light band visible that was present in both $lum^{+/+}$ and $lum^{-/-}$ presumably a cross reactive band and not a partially expressed protein in the $lum^{-/-}$ given that it was the highest MW band (78 kD) observed in the analysis. Using GAPDH to normalize, the amount of LUM protein increased approximately four fold from P0 to adult (Fig. 1J).

### 3.2 Lumican deficient mice exhibit significant perinatal death and increased myocardial area

To determine the role of LUM in the myocardium of the developing murine heart we utilized LUM deficient mice ($lum^{-/-}$) [18]. Since the time of original report, the $lum^{-/-}$ mice that were on a CD1 background have been crossed into the C57BL/6 a minimum of 10 generations and are now on a pure C57BL/6 genetic background. On the C57BL/6 background the $lum^{-/-}$ mice exhibited a significant amount of perinatal death not previously reported on the CD1 background (S. Fig. 1). Mendialian genetics of fetal staged embryos (E17.5) from heterozygous $lum^{+/-}$ matings revealed that there was no deviation from the expected 1:2:1 ratio of WT:Het:KO (S. Fig. 1) however at P0 and 1 month the Mendialian ratios were significantly altered with approximately 50% of $lum^{-/-}$ mice dying within the first 24 hours after birth.

Frontal sections of E17.5 hearts from $lum^{-/-}$ and WT littermates showed no morphological differences within ventricular myocardium (n=9 WT; n=10 $lum^{-/-}$ ; data not shown). However at P0 in hearts from $lum^{-/-}$ mice there was increased myocardial area and decreased ventricular lumen when compared to WT (Fig. 2A, B; n=7 WT, n=9 $lum^{-/-}$ 90% penetrance). Quantification of the myocardium showed a significant increase in myocardial area in $lum^{-/-}$ hearts (Fig. 2C; $P < 2.0 \times 10^{-6}$). Three-dimensional (3D) reconstructions using Amira™ software also illustrated the increased myocardial area and concomitant reduction in ventricular lumen throughout the entire depth of the heart (Fig. 2D–F; purple-myocardium, cyan-lumen). Quantitative assessment using data from 3D reconstructions

revealed statistical significance in the *lum*$^{-/-}$ P0 hearts (n=3 *lum*$^{-/-}$ ; $P$ <0.02; n=2 WT); in addition 3D of lumen also demonstrated that the reduction in RV and LV lumen volume was significantly reduced in *lum*$^{-/-}$ hearts compared to WT (P <0.02). At 1 mo the viable *lum*$^{-/-}$ hearts fell into two categories, hearts that exhibited a statistically significant increase in myocardial area (n=5/8 *lum*$^{-/-}$ 62%, $P < 1.6 \text{ X } 10^{-6}$ ; n=5 WT) and hearts that appeared within a normal range with respect to ventricular myocardial area denoted *lum*$^{-/-}$ NH (Non-Hypertrophic; n=3/8 *lum*$^{-/-}$ 38%; n=5 WT) (Fig. 2G–I). The morphological changes in the *lum*$^{-/-}$ hearts were the result of increased myocardial area and concomitant reduction in ventricular lumen. The percentage of mice that show the increased myocardial area at one month is reduced compared to P0 and is likely impacted by the survival rate of *lum*$^{-/-}$ after birth.

### 3.3 Increased myocardial area in Lumican deficient hearts is due to cardiomyocyte hypertrophy

An increase in ventricular myocardial area could be due to an increase in cell number, i.e. hyperplasia or an increase in cell size i.e. hypertrophy. The proliferation rate of ventricular cells in the *lum*$^{-/-}$ and WT littermates was evaluated using phosphoHistone H3 (PHH3) IHC at E17.5 (n=2 WT, n=3 *lum*$^{-/-}$), E18.5 (n=3 WT, n=4 *lum*$^{-/-}$) and P0 (n=5 WT, n=3 *lum*$^{-/-}$). At these time points there was no significant change in the proliferative rate of cells within the right ventricle (RV), septum (S) or left ventricle (LV) (S. Fig. 2A–C) of *lum*$^{-/-}$ hearts compared to WT littermates. Given that the increased ventricular area phenotype was acquired between E17.5 and birth, these data suggest that the increased myocardial area in *lum*$^{-/-}$ was not due to changes in the proliferative rate (i.e. hyperplasia) of any of the cell-types within the ventricular walls and septum compared to WT littermates.

The size of cardiomyocytes from *lum*$^{-/-}$ and WT littermates were examined at P0, 1 mo and 4 mo. An antibody recognizing the cardiomyocyte protein α-sarc was utilized to identify cardiomyocytes within the ventricles of *lum*$^{-/-}$ and WT hearts and cell boundaries were outlined using a laminin antibody (Fig. 3A, B, E, F, I, J). The size of the cardiomyocytes was determined by measuring the widest part of α-sarc positive cells, in sections from *lum*$^{-/-}$ and WT hearts (Fig. 3). Cardiomyocytes from the LV at P0 displayed a range in diameter from approximately 2-18μm (Fig. 3C; n=4 WT, n=4 *lum*$^{-/-}$). On the Y-axis the percentage of cardiomyocytes from the LV corresponds to the range of cardiomyocyte cell size (in 1.5μm intervals) on the X-axis (Fig. 3C). There was an increase in the number of cardiomyocytes in the larger cell size ranges in the *lum*$^{-/-}$ hearts compared to WT as denoted by the shift in black bars to the right (*lum*$^{-/-}$) compared to grey bars (WT). In addition the average size of the cardiomyocytes was significantly larger in the *lum*$^{-/-}$ compared to WT (Fig. 3D; 8.9μm versus 7.8μm, $P< 1.1 \text{ X } 10^{-8}$). Myocardial cell size was also measured in the RV and ventricular septum (S. Fig. 3). The cardiomyocytes within these regions of the P0 *lum*$^{-/-}$ heart also showed a similar shift in larger cell size ranges as well as a statistical increase in the average myocardial cell size. Myocardial diameters were also measured in surviving 1 mo *lum*$^{-/-}$ mice with increased muscle area (Fig. 3E–H; n=5 WT, n=5 *lum*$^{-/-}$). At this age cardiomyocytes were identified based on their rod-shaped phenotype, α-sarc positive staining and cell boundaries were highlighted using IHC for laminin (Fig. 3E, F). Cardiomyocytes from *lum*$^{-/-}$ 1 mo hearts had a greater number of

larger sized cells in the RV, S (S. Fig. 3) and LV denoted by the shift to the right in *lum*$^{-/-}$ (black) versus WT (grey) bars (Fig. 3G). In addition, the average cardiomyocyte cell size was larger in the *lum*$^{-/-}$ (22μm) compared to WT (Fig. 3H; 16μm, $P<2.3 \times 10^{-5}$) at 1 month. Similar data was also obtained for adult *lum*$^{-/-}$ (Fig. 3I–L; 4 mo, n=3 WT, n= 3 *lum*$^{-/-}$) cardiomyocytes, there was a shift to the right with a higher percentage of *lum*$^{-/-}$ cardiomyocytes in the larger sizes, including > 10% within the largest size ranges where no WT cardiomyocytes were represented (Fig. 3K). The overall average diameter was also significantly increased in adult (4 mo) *lum*$^{-/-}$ (25.6μm) compared to WT (21.1μm) (Fig. 3L; $P < 9.5 \times 10^{-6}$).

Therefore, the similar rate of cell proliferation and the statistically significant increase in myocardial cell size of the *lum*$^{-/-}$ compared to the WT at all postnatal stages evaluated suggested that the increased muscle area in the *lum*$^{-/-}$ hearts is due to cardiomyocyte hypertrophy rather than hyperplasia.

### 3.4 Lumican deficient murine hearts display reduced levels of higher molecular weight βand γforms of Collagen I compared to wild type littermates

Since lumican modifies collagen I fiber assembly in other tissues [10–13] we used immunolocalization to determine the spatiotemporal expression of collagenα1(I) in ventricular myocardium from *lum*$^{-/-}$ and WT littermates. These studies showed a dramatic increase in collagenα1(I) immunolocalization around cardiomyocytes (pericellular/ myomysial) from P0 to 1 month (FIG. 4A, D, G, J, solid arrowheads), the developmental window when cardiomyocytes differentiate into their rod-shaped phenotype. While detectable in multiple fixatives, frozen sections dramatically improved sensitivity at late gestational and early post-natal time-points. In addition to the pericellular staining, collagenα1(I) was present in the perimysial ECM (sheath ECM/ interstitial ECM) that by one month serves to bundle working groups of cardiomyocytes (Fig. 4A, D, G, J, M, P, open arrowheads). Of note, there was less IHC for collagenα1(I) in the sheath ECM forming towards the lumen (L) at P0 in *lum*$^{-/-}$ hearts (**A, D**). For collagenα1(I) the staining intensity was similar in the pericellular (solid arrowheads) and perimysial (open arrowheads) ECM for both WT and *lum*$^{-/-}$ hearts at all stages examined.

The collagen fibrils from adult WT and *lum*$^{-/-}$ hearts were examined using transmission electron microscopy (Fig. 4S–U). In *lum*$^{-/-}$ hearts the collagen fibrils exhibited a larger diameter ($P< 2.34 \times 10^{-33}$) and appeared less electron dense than in WT hearts. The distribution of collagen fibrils (Fig. 4U) revealed more collagen fibrils with larger diameter sizes in the *lum*$^{-/-}$ hearts (Fig. 4U, black bars) compared to WT (Fig. 4U, grey bars).

Total mature insoluble collagen content was measured using the hydroxyproline assay. The *lum*$^{-/-}$ hearts had reduced levels of insoluble collagen (mature cross-linked fibrillar collagen) compared to WT (Fig. 4V, *lum*$^{-/-}$ 1.30 +/− 0.05 μg hydroxyproline/mg dry wt; WT, 1.60 +/− 0.07 μg hydroxyproline/mg dry wt; $P < 0.05$; n=9).

Western blots of collagenα1(I) using 3–8% gradient gels on heart extracts from P0 (Fig. 5A) and 1 mo (Fig. 5D) *lum*$^{-/-}$ and WT littermates were performed (P0: n=2 WT, n=3 *lum*$^{-/-}$ ; 1 mo: n=2 WT, n=2 *lum*$^{-/-}$). Images shown are from heart extracts of one WT and two *lum*$^{-/-}$

littermates per stage; each sample was loaded in triplicate at 50, 25 and 12.5 μg of total protein respectively and denoted by the triangle above the lanes (Fig. 5A, D). Western blots for collagenα1(I) revealed a reduction in the γcomponents of collagen at approximately 300kD (Fig. 5A, D, solid arrowhead) in the *lum*$^{-/-}$ compared to WT mice. The γ 300kD band is consistent with the covalent cross-linkage of 3 processed collagen peptides; while the β bands share the MW of two covalently cross-linked peptides. The α peptides, represent non-cross-linked peptides are visible in three separate MW bands depending on the processing of the N or C terminal propeptide that are cleaved prior to collagen fiber assembly. In essence the multiple collagen bands (α, β and γ) may be considered as a snapshot of collagen fibril assembly in the WT compared to *lum*$^{-/-}$ hearts. In this study we observed the ratio of β and γ forms (blue boxes, solid and open arrowheads) compared to αpolypeptides (red boxes) was significantly altered at P0 (Fig. 5C) and 1 mo (Fig. 5F) in the *lum*$^{-/-}$ compared to WT hearts (P0, $P < 0.02$; 1 mo, $P < 0.02$ By 1 mo the total amount of soluble collagen was also significantly reduced in the *lum*$^{-/-}$ mice ($P < 0.02$; Fig. 5E).

### 3.5 The class I SLRP decorin high molecular weight GAG-containing forms are reduced in hearts from the lumican deficient mice

Since decorin (DCN) is also involved in collagen assembly and its expression increases from embryonic to adult cardiac fibroblasts [22] we evaluated the spatiotemporal expression of decorin in the *lum*$^{-/-}$ compared to WT hearts. DCN expression colocalized with collagenα1(I) at all developmental stages examined (Fig. 4B, C, E, F, H, I, K, L, N, O, Q, R). Similar to collagenα1(I) there was a dramatic increase in immunolocalization of DCN at 1 mo in both the pericellular ECM around cardiomyocytes (Fig. 4H, K solid arrows) as well as the perimysial ECM (Fig. 4H, K open arrows). DCN appeared to be in greater abundance in the perimysial/sheath ECM compared to the pericellular cardiomyocyte ECM whereas collagenα1(I) showed a similar immunoreactivity in these ECM structures (Fig. 4G–R). By 1 mo there appeared to be a reduction in DCN in the *lum*$^{-/-}$ ventricular myocardium compared to WT with the most prominent differences in the pericellular cardiomyocyte ECM (Fig. 4H, K, solid arrows). The apparent reduction in DCN localization was also maintained in the adult (4 mo) *lum*$^{-/-}$ hearts (Fig. 4N, Q, solid arrows). Western blots from 4–12% gradient gels of P0 (Fig. 6A; n=2 WT, n=3 *lum*$^{-/-}$) and 1 mo (Fig. 6D; n=2 WT, n=2 *lum*$^{-/-}$) heart extracts revealed a reduction in the higher molecular weight (GAG-containing) forms of decorin (Fig. 6A, D, solid and open arrowheads, blue boxes) in *lum*$^{-/-}$ compared to WT littermates. Extracts from one WT and two *lum*$^{-/-}$ hearts from the same litter are shown at P0 and 1 mo; each sample was loaded in triplicate using 50, 25 and 12.5 μg respectively and denoted by the triangle above the lanes. In P0 extracts, a band at approximately 30kD, consistent with the core polypeptide was visible. A triplet just below the 50kD marker (Fig. 6A, red boxes) that represents nonglycanated decorin forms that have heterogeneous oligosaccharide chains [23–25] was also present. The higher MW bands at 75kD (Fig. 6A, D, solid arrowhead) and 95kD (Fig. 6A, open arrowhead) were visible at P0 and have been previously characterized by others [23] to shift to 50 kD after chondroitinase ABC digestion and are further digested with PNGase F in a protein deglycosylation mix to a core band at 30 kD [24]. In the *lum*$^{-/-}$ heart extracts the reduction of higher molecular weight (GAG) form was statistically significant at 1 mo (Fig. 6D, blue box, E). There was also a relative increase in the core polypeptide (30kD) at both P0 and 1 mo (Fig. 6A, C, D, F, red boxes) in the

*lum*$^{-/-}$ hearts. Collectively this resulted in a significant difference in the ratio of higher MW decorin (blue boxes) compared to the lower MW forms 30kD plus 50kD bands (Fig. 6A, D, red boxes) at both P0 (Fig. 6C, $P$ <0.02) and 1 mo in *lum*$^{-/-}$ hearts (Fig. 6F, $P$ < 0.04). Of note, in 1mo hearts of both WT and *lum*$^{-/-}$ the 95 kD form of DCN found in the P0 hearts (Fig. 6A, open arrowhead 95kD) was not detected however the 75 band was clearly visible at these later stages.

## 4. Discussion

Here we presented the first evidence that LUM, a class II SLRP, may be required within the ventricular myocardium to mediate assembly of the collagen-rich ECM during cardiac development. The lumican deficient hearts appear morphologically normal in late fetal stages of development, however after birth there is an increase in myocardial area due to increased cardiomyocyte size, presumably due to an in insufficient pericellular ECM (Fig. 7). In mice, the majority of collagen-rich pericellular ECM is acquired postnatally as cardiomyocytes differentiate into their block-shaped phenotype. Since a significant percentage of lumican deficient mice died at birth, this suggests the early ECM architecture of the heart may also require LUM to control cardiomyocyte size and/or contractile function. The proper formation of the myocardial ECM is critical for maintaining cardiomyocyte alignment, mechanical coupling and structural integrity. LUM, like other SLRPs [26–29] may also be required to regulate growth factor availability and mediate chemokine response [24] allowing the heart to adapt to pathophysiological stimuli. We speculate that LUM deficient cardiomyocytes are unable to withstand the increased biomechanical force after birth and this additional stress results in cardiomyocyte hypertrophy. The increase in myocardial area and concomitant reduction of the ventricular lumen may severely impact cardiac output (stroke volume) in LUM deficient mice at birth and contribute to the significant perinatal death observed.

There is increasing evidence that cardiac fibroblasts produce the ECM components that regulate cardiomyocyte phenotype and function [30] suggesting that fibroblast-cardiomyocyte interaction is required for proper pericellular and sheath ECM assembly. This is consistent with our study where LUM was localized to stellate shaped cells adjacent to α-sarc actin positive cardiomyocytes in fetal, early postnatal and adult murine hearts. Isolated cardiac fibroblasts from embryonic and adult hearts express lumican mRNA, albeit adult fibroblasts express a 4-fold increase compared to embryonic cardiac fibroblasts [22]. Although there are multiple origins of cardiac fibroblasts in the murine heart, the spatiotemporal expression of lumican overlaps with areas subjected to maximal biomechanical force therefore we speculate lumican production is more dependent on spatiotemporal aspects within the heart rather than fibroblast origin [31].

Previous studies using the LUM deficient mice have established its role in crosslinking collagen I fibrils during ECM assembly of several tissues. Electron microscopy of the lumican deficient cornea, skin and tendon also show irregular collagen fibril contours as well as increased fibril diameter [1532]. Our data is consistent with lumican playing a role in early collagen fibril assembly [33]. However data presented here also suggest LUM facilitates intra and/or intermolecular crosslinking within the collagenα1(I) containing

subunit, since the higher molecular weight β and γ bands were reduced in the lumican deficient hearts at P0 and 1 month. Since DCN levels are altered in lum$^{-/-}$ hearts and DCN binds to procollagen [34] this gives further indication that SLRPs may facilitate early collagen subunit intra and intermolecular cross-linking, perhaps by allowing conformational changes that increase lysyl oxidase activity. Controlled assembly of collagen fibrils was also altered by changes in intermolecular cross-linking of tendons from mice deficient in the class II SLRP, fibromodulin [35]. The fact that DCN forms were reduced within the lumican deficient hearts suggests collagen assembly is tightly controlled at multiple levels and LUM expression is essential for appropriate post-translational modifications of other SLRPs involved in collagen fiber formation. Abnormal DCN glycosylation is a major mechanistic cause of the defective skin seen in Ehlers- Danlos syndrome [36], therefore the fact that GAG-DCN is reduced in LUM deficient hearts may, in and of itself, significantly alter ECM architecture. Although the precise role of sulfated GAGs on SLRPs is not clear they regulate matrix hydration [37] and allow tethering between adjacent collagen fibrils [3839]. Of note, this study revealed that at P0, in early stages of collagen assembly in the developing heart, there were two GAG-containing forms of decorin, while at 1 mo, only the lower MW GAG-decorin was detected. A shift to the higher MW GAG-decorin was also observed in murine hearts subjected to pressure overload [40]. Since collagen assembly occurs at a rapid rate in the first month of postnatal life and in response to pressure overload, perhaps the elongated (higher MW form of) GAG-decorin may work coordinately with LUM to facilitate early stages of collagen fibril assembly required to adapt the ECM architecture to increased biomechanical force. The potential cross-talk between LUM and DCN is further complicated by the fact that DCN is cleaved by several ECM proteases [41–44] and others also report bands consistent with its dimerization [23], facets of posttranslational modification that are likely impacted by altered LUM levels. Collectively the ECM architecture may be profoundly altered in lumican deficient hearts, due not only to the loss of LUM but also to changes in protein levels of other collagen fiber components including the alteration of posttranslational modifications. Therefore further studies utilizing the LUM deficient mice will likely unveil additional ECM events that are coordinately regulated to ensure appropriate collagen assembly.

The fact that LUM as well as the class I SLRP decorin, are upregulated in response to pathophysiological stimuli such as aortic banding [45] and RV pressure overload [40] indicates that SLRP expression enhances structural integrity of the murine heart. Additional studies demonstrated that the 7-fold increase in lumican expression after aortic banding was decreased again 14 days after debanding [24]. *In vitro* mechanical stretch of rat cardiac fibroblasts also induced lumican mRNA [45]. In rat ischemic and reperfused hearts, lumican expression was increased and localized in collagen fibers of fibrotic lesions. Recently, cardiac biopsies from patients with end-stage heart failure revealed an increase in lumican protein and mRNA levels compared to controls [45]. Notably the upregulation of lumican may not necessarily contribute to the disease progression, but may provide a compensatory function in an effort to stabilize the myocardial tissue during conditions of pressure overload. For example, CXCR5 deficient mice show significantly reduced levels of lumican, and other collagen-binding SLRPs; the decrease in SLRP expression correlates with an increase in mortality in these mice during pressure overload [46]. A role for lumican in

stabilizing the ventricular myocardium in response to increased mechanical force is consistent with its developmental role presented here where loss of lumican resulted in an increase in mortality and cardiomyocyte hypertrophy. These studies suggest that lumican may play a critical role in the cardiac ECM architecture both in normal development and also for adaptation of the heart in response to changes in biomechanical stimuli during conditions of disease or stress.

In addition to its structural role in maintaining tissue integrity, lumican may also sequester growth factors and interact with receptors similar to other SLRPs [26, 27, 29, 47, 48]. Recent experiments demonstrate that exogenous addition of recombinant glycosylated lumican to rat cardiac fibroblasts increases mRNA of TGFβ1 and phosphorylation of downstream mediator Smad3. Moreover there is a 1.9 fold increase in collagenα2(I) mRNA, a 1.8 fold increase in LOX mRNA, indicating that an increase in lumican expression can upregulate additional ECM components involved in collagen fiber assembly and stability[45]. The observation that LUM deficiency impacted collagenα1(I) levels and cross-linking, as well as DCN levels and GAG-DCN modifications, may indicate loss of signaling functions of LUM. Therefore the postnatal cardiomyocyte hypertrophy observed in the *lum*$^{-/-}$ mice, and the fact that postnatal cardiomyocyte differentiation mirrors pericellular ECM assembly, may be indicative of the dual role of lumican in the murine heart; a component of the collagen-rich ECM architecture and also a key signaling molecule involved in adaptation to increased biomechanical forces by regulating the complex process of collagen fiber assembly.

This developmental study as well as previous work that illustrates an upregulation of lumican in in response to an increase in biomechanical stimuli of the heart, suggests lumican and potentially other SLRPS may serve a critical role in the dynamic cardiovascular ECM during development and in disease. Additional investigation into the role of lumican should advance our understanding of how changes in biomechanical forces translate into dramatic alterations within the ECM architecture of the mammalian heart. In addition, a better understanding of the regulatory mechanisms involved in collagen assembly is fundamental to developing strategies to reverse or to prevent excess collagen deposition in pathophysiological conditions that contribute to cardiac dysfunction. Given the dual role of SLRPs in tissue integrity and cell signaling, further examination into the role of SLRPs may also yield novel therapeutic targets and/or biomarkers for patients with cardiovascular disease.

## Supplementary Material

Refer to Web version on PubMed Central for supplementary material.

## Acknowledgements

The authors would like to thank Aimee Phelps for her histological expertise. This work was supported by The American Heart Association; 10SDG2610168 (CBK), NIH R01 HL121382 (CBK) and NIH-NIGMS P30 GM103342; 13GRNT16500000 (ADB) and the VA Merit Award: 1I01BX001385-01A1 (ADB); NIH EY11654 (SC).

## Abbreviations

| | |
|---|---|
| **ECM** | extracellular matrix |
| **LUM** | lumican |
| **SLRP** | small leucine-rich proteoglycan |
| **DCN** | decorin |
| **WT** | wild type |
| **P0** | postnatal day 0 |
| **1 mo** | 1 month |
| **IHC** | immunohistochemistry |
| **LV** | left ventricle |
| **RV** | right ventricle |
| **NH** | non-hypertrophic |
| **GAG** | glycosaminoglycan |

## References


1. Dorn GW 2nd, Robbins J, Sugden PH. Phenotyping hypertrophy: eschew obfuscation. Circ Res. 2003; 92:1171–1175. [PubMed: 12805233]
2. Levy D, Garrison RJ, Savage DD, Kannel WB, Castelli WP. Prognostic implications of echocardiographically determined left ventricular mass in the Framingham Heart Study. N Engl J Med. 1990; 322:1561–1566. [PubMed: 2139921]
3. Evans SM, Yelon D, Conlon FL, Kirby ML. Myocardial lineage development. Circ Res. 2010; 107:1428–1444. [PubMed: 21148449]
4. Klug MG, Soonpaa MH, Koh GY, Field LJ. Genetically selected cardiomyocytes from differentiating embronic stem cells form stable intracardiac grafts. J Clin Invest. 1996; 98:216–224. [PubMed: 8690796]
5. Goldsmith EC, Borg TK. The dynamic interaction of the extracellular matrix in cardiac remodeling. Journal of cardiac failure. 2002; 8:S314–S318. [PubMed: 12555138]
6. Terracio L, Rubin K, Gullberg D, Balog E, Carver W, Jyring R, et al. Expression of collagen binding integrins during cardiac development and hypertrophy. Circ Res. 1991; 68:734–744. [PubMed: 1835909]
7. Goldsmith EC, Bradshaw AD, Zile MR, Spinale FG. Myocardial fibroblast-matrix interactions and potential therapeutic targets. J Mol Cell Cardiol. 2014; 70:92–99. [PubMed: 24472826]
8. Miller AD, Tyagi SC. Mutation in collagen gene induces cardiomyopathy in transgenic mice. J Cell Biochem. 2002; 85:259–267. [PubMed: 11948682]
9. Callewaert B, Malfait F, Loeys B, De Paepe A. Ehlers-Danlos syndromes and Marfan syndrome. Best practice & research Clinical rheumatology. 2008; 22:165–189. [PubMed: 18328988]
10. Byers PH. Ehlers-Danlos syndrome: recent advances and current understanding of the clinical and genetic heterogeneity. The Journal of investigative dermatology. 1994; 103:47S–52S. [PubMed: 7963684]
11. Raff ML, Byers PH. Joint hypermobility syndromes. Current opinion in rheumatology. 1996; 8:459–466. [PubMed: 8941450]
12. Chakravarti S. The cornea through the eyes of knockout mice. Experimental eye research. 2001; 73:411–419. [PubMed: 11825014]

13. Iozzo RV, Moscatello DK, McQuillan DJ, Eichstetter I. Decorin is a biological ligand for the epidermal growth factor receptor. J Biol Chem. 1999; 274:4489–4492. [PubMed: 9988678]
14. Tingbo MG, Pedersen ME, Kolset SO, Enersen G, Hannesson KO. Lumican is a major small leucine-rich proteoglycan (SLRP) in Atlantic cod (Gadus morhua L.) skeletal muscle. Glycoconjugate journal. 2012; 29:13–23. [PubMed: 22124673]
15. Jepsen KJ, Wu F, Peragallo JH, Paul J, Roberts L, Ezura Y, et al. A syndrome of joint laxity and impaired tendon integrity in lumican- and fibromodulin-deficient mice. J Biol Chem. 2002; 277:35532–35540. [PubMed: 12089156]
16. Chakravarti S, Zhang G, Chervoneva I, Roberts L, Birk DE. Collagen fibril assembly during postnatal development and dysfunctional regulation in the lumican-deficient murine cornea. Dev Dyn. 2006; 235:2493–2506. [PubMed: 16786597]
17. Beecher N, Chakravarti S, Joyce S, Meek KM, Quantock AJ. Neonatal development of the corneal stroma in wild-type and lumican-null mice. Invest Ophthalmol Vis Sci. 2006; 47:146–150. [PubMed: 16384956]
18. Chakravarti S, Magnuson T, Lass JH, Jepsen KJ, LaMantia C, Carroll H. Lumican regulates collagen fibril assembly: skin fragility and corneal opacity in the absence of lumican. J Cell Biol. 1998; 141:1277–1286. [PubMed: 9606218]
19. Kern CB, Norris RA, Thompson RP, Argraves WS, Fairey SE, Reyes L, et al. Versican proteolysis mediates myocardial regression during outflow tract development. Dev Dyn. 2007; 236:671–683. [PubMed: 17226818]
20. Dupuis LE, McCulloch DR, McGarity JD, Bahan A, Wessels A, Weber D, et al. Altered versican cleavage in ADAMTS5 deficient mice; a novel etiology of myxomatous valve disease. Dev Biol. 2011; 357:152–164. [PubMed: 21749862]
21. Bradshaw AD, Reed MJ, Sage EH. SPARC-null mice exhibit accelerated cutaneous wound closure. The journal of histochemistry and cytochemistry : official journal of the Histochemistry Society. 2002; 50:1–10. [PubMed: 11748289]
22. Ieda M, Tsuchihashi T, Ivey KN, Ross RS, Hong TT, Shaw RM, et al. Cardiac fibroblasts regulate myocardial proliferation through beta1 integrin signaling. Dev Cell. 2009; 16:233–244. [PubMed: 19217425]
23. Li Y, Liu Y, Xia W, Lei D, Voorhees JJ, Fisher GJ. Age-dependent alterations of decorin glycosaminoglycans in human skin. Scientific reports. 2013; 3:2422. [PubMed: 23939413]
24. Engebretsen KV, Waehre A, Bjornstad JL, Skrbic B, Sjaastad I, Behmen D, et al. Decorin, lumican, and their GAG chain-synthesizing enzymes are regulated in myocardial remodeling and reverse remodeling in the mouse. J Appl Physiol (1985). 2013; 114:988–997. [PubMed: 23412898]
25. Carrino DA, Sorrell JM, Caplan AI. Age-related changes in the proteoglycans of human skin. Archives of biochemistry and biophysics. 2000; 373:91–101. [PubMed: 10620327]
26. Chen S, Birk DE. The regulatory roles of small leucine-rich proteoglycans in extracellular matrix assembly. The FEBS journal. 2013; 280:2120–2137. [PubMed: 23331954]
27. Moreth K, Iozzo RV, Schaefer L. Small leucine-rich proteoglycans orchestrate receptor crosstalk during inflammation. Cell Cycle. 2012; 11:2084–2091. [PubMed: 22580469]
28. Iozzo RV, Karamanos N. Proteoglycans in health and disease: emerging concepts and future directions. The FEBS journal. 2010; 277:3863. [PubMed: 20812984]
29. Kalamajski S, Oldberg A. The role of small leucine-rich proteoglycans in collagen fibrillogenesis. Matrix Biol. 2010; 29:248–253. [PubMed: 20080181]
30. Banerjee I, Yekkala K, Borg TK, Baudino TA. Dynamic interactions between myocytes, fibroblasts, and extracellular matrix. Ann N Y Acad Sci. 2006; 1080:76–84. [PubMed: 17132776]
31. Lajiness JD, Conway SJ. Origin, development, and differentiation of cardiac fibroblasts. J Mol Cell Cardiol. 2014; 70:2–8. [PubMed: 24231799]
32. Chakravarti S. Functions of lumican and fibromodulin: lessons from knockout mice. Glycoconjugate journal. 2002; 19:287–293. [PubMed: 12975607]
33. Ezura Y, Chakravarti S, Oldberg A, Chervoneva I, Birk DE. Differential expression of lumican and fibromodulin regulate collagen fibrillogenesis in developing mouse tendons. J Cell Biol. 2000; 151:779–788. [PubMed: 11076963]

34. Keene DR, San Antonio JD, Mayne R, McQuillan DJ, Sarris G, Santoro SA, et al. Decorin binds near the C terminus of type I collagen. J Biol Chem. 2000; 275:21801–21804. [PubMed: 10823816]
35. Kalamajski S, Liu C, Tillgren V, Rubin K, Oldberg A, Rai J, et al. Increased C-telopeptide crosslinking of tendon type I collagen in fibromodulin-deficient mice. J Biol Chem. 2014; 289:18873–18879. [PubMed: 24849606]
36. Gotte M, Kresse H. Defective glycosaminoglycan substitution of decorin in a patient with progeroid syndrome is a direct consequence of two point mutations in the galactosyltransferase I (beta4GalT-7) gene. Biochemical genetics. 2005; 43:65–77. [PubMed: 15859521]
37. Liu CY, Birk DE, Hassell JR, Kane B, Kao WW. Keratocan-deficient mice display alterations in corneal structure. J Biol Chem. 2003; 278:21672–21677. [PubMed: 12665512]
38. Henninger HB, Maas SA, Underwood CJ, Whitaker RT, Weiss JA. Spatial distribution and orientation of dermatan sulfate in human medial collateral ligament. Journal of structural biology. 2007; 158:33–45. [PubMed: 17150374]
39. Lewis PN, Pinali C, Young RD, Meek KM, Quantock AJ, Knupp C. Structural interactions between collagen and proteoglycans are elucidated by three-dimensional electron tomography of bovine cornea. Structure. 2010; 18:239–245. [PubMed: 20159468]
40. Waehre A, Vistnes M, Sjaastad I, Nygard S, Husberg C, Lunde IG, et al. Chemokines regulate small leucine-rich proteoglycans in the extracellular matrix of the pressure-overloaded right ventricle. J Appl Physiol (1985). 2012; 112:1372–1382. [PubMed: 22345433]
41. Carrino DA, Onnerfjord P, Sandy JD, Cs-Szabo G, Scott PG, Sorrell JM, et al. Age-related changes in the proteoglycans of human skin. Specific cleavage of decorin to yield a major catabolic fragment in adult skin. J Biol Chem. 2003; 278:17566–17572. [PubMed: 12621051]
42. Imai K, Hiramatsu A, Fukushima D, Pierschbacher MD, Okada Y. Degradation of decorin by matrix metalloproteinases: identification of the cleavage sites, kinetic analyses and transforming growth factor-beta1 release. The Biochemical journal. 1997; 322(Pt 3):809–814. [PubMed: 9148753]
43. Svensson L, Heinegard D, Oldberg A. Decorin-binding sites for collagen type I are mainly located in leucine-rich repeats 4–5. J Biol Chem. 1995; 270:20712–20716. [PubMed: 7657652]
44. Schonherr E, Broszat M, Brandan E, Bruckner P, Kresse H. Decorin core protein fragment Leu155-Val260 interacts with TGF-beta but does not compete for decorin binding to type I collagen. Archives of biochemistry and biophysics. 1998; 355:241–248. [PubMed: 9675033]
45. Engebretsen KV, Lunde IG, Strand ME, Waehre A, Sjaastad I, Marstein HS, et al. Lumican is increased in experimental and clinical heart failure, and its production by cardiac fibroblasts is induced by mechanical and proinflammatory stimuli. The FEBS journal. 2013; 280:2382–2398. [PubMed: 23480731]
46. Waehre A, Halvorsen B, Yndestad A, Husberg C, Sjaastad I, Nygard S, et al. Lack of chemokine signaling through CXCR5 causes increased mortality, ventricular dilatation and deranged matrix during cardiac pressure overload. PloS one. 2011; 6:e18668. [PubMed: 21533157]
47. Nikitovic D, Katonis P, Tsatsakis A, Karamanos NK, Tzanakakis GN. Lumican, a small leucinerich proteoglycan. IUBMB life. 2008; 60:818–823. [PubMed: 18949819]
48. Iozzo RV, Schaefer L. Proteoglycans in health and disease: novel regulatory signaling mechanisms evoked by the small leucine-rich proteoglycans. The FEBS journal. 2010; 277:3864–3875. [PubMed: 20840584]

## Highlights

- Mice deficient in lumican exhibit significant perinatal mortality.
- Lumican deficiency leads to cardiomyocyte hypertrophy
- Lumican is required for normal GAG modification of decorin.
- The pericellular ECM of cardiomyocytes requires lumican production by fibroblasts.
- Collagen fibril assembly is altered in lumican deficient hearts.

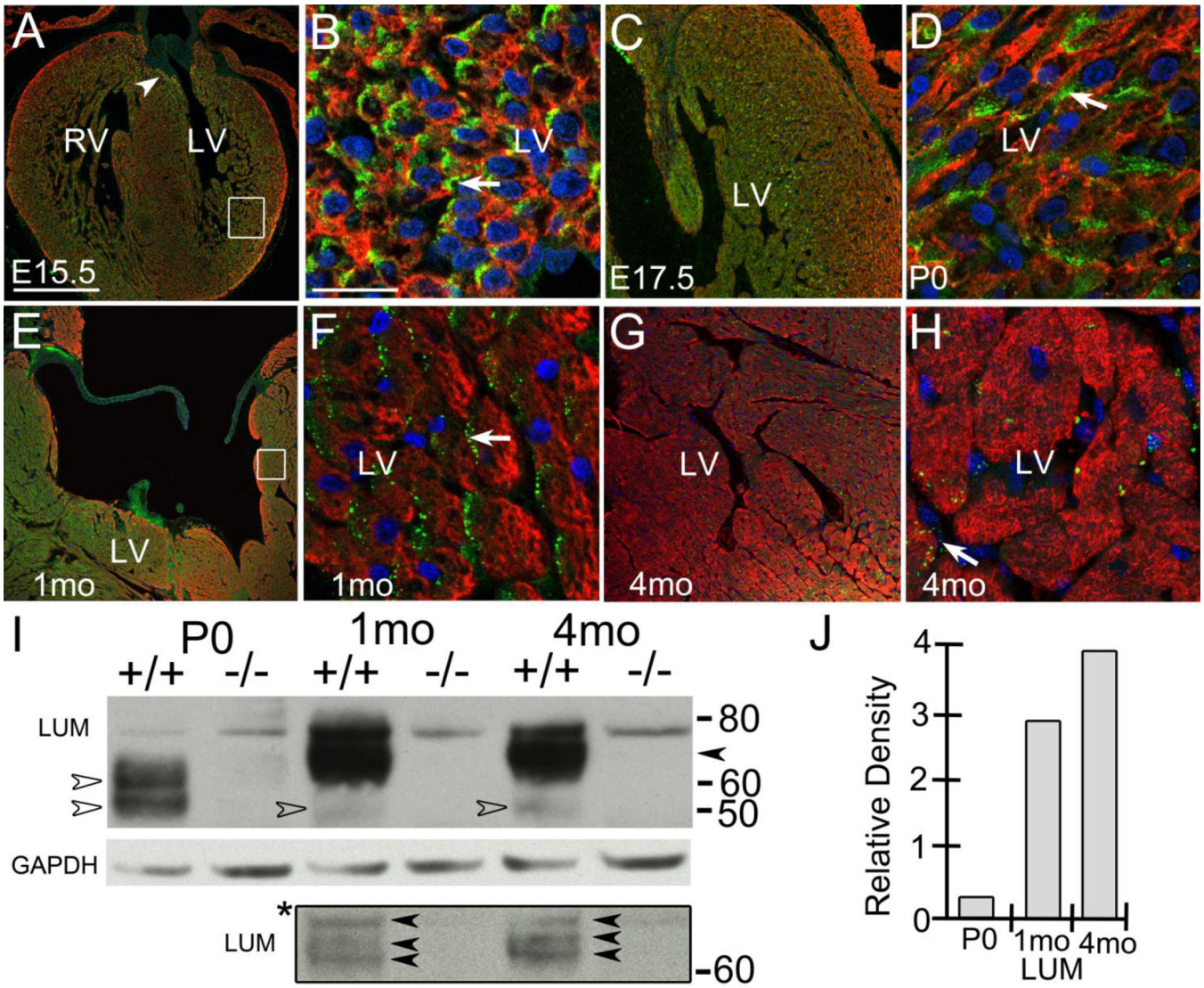


**Figure 1. The SLRP proteoglycan lumican was expressed by non-cardiomyocytes in the murine heart**

Immunolocalization of lumican (LUM, green) at embryonic day 15.5 (E15.5), (A, B), E17.5 (C), P0 (D), 1 month (1 mo) (E, F) and adult (4 mo) (G, H). A, arrowhead- expression subjacent to valve mesenchyme; box in A magnified in B. LUM was associated with α-sarcomeric actin (red) negative cells (B, D, F, arrows). Box in E, shown in higher magnification in F. Blue- propidium iodide. Magnification Bars: A= 250 μm and applies to E, G; B = 10 μm and applies to D, F; C = 125 μm; H= 50 μm. Western blot of LUM in WT mice at P0, 1mo and 4 mo (I). Open arrows denote predominant P0 forms at 50kD and 60kD. * bounded box-different exposure of gel above. Solid arrows denote MW bands 60–75 kD bands in 1mo and 4mo hearts absent in P0 samples. Solid arrow denotes 65–75 MW bands in 1 mo and 4 mo hearts; +/+, wild type heart lysates; −/−, lum$^{-/-}$ heart lysates; GAPDH-loading control; RV- right ventricle, LV- left ventricle.

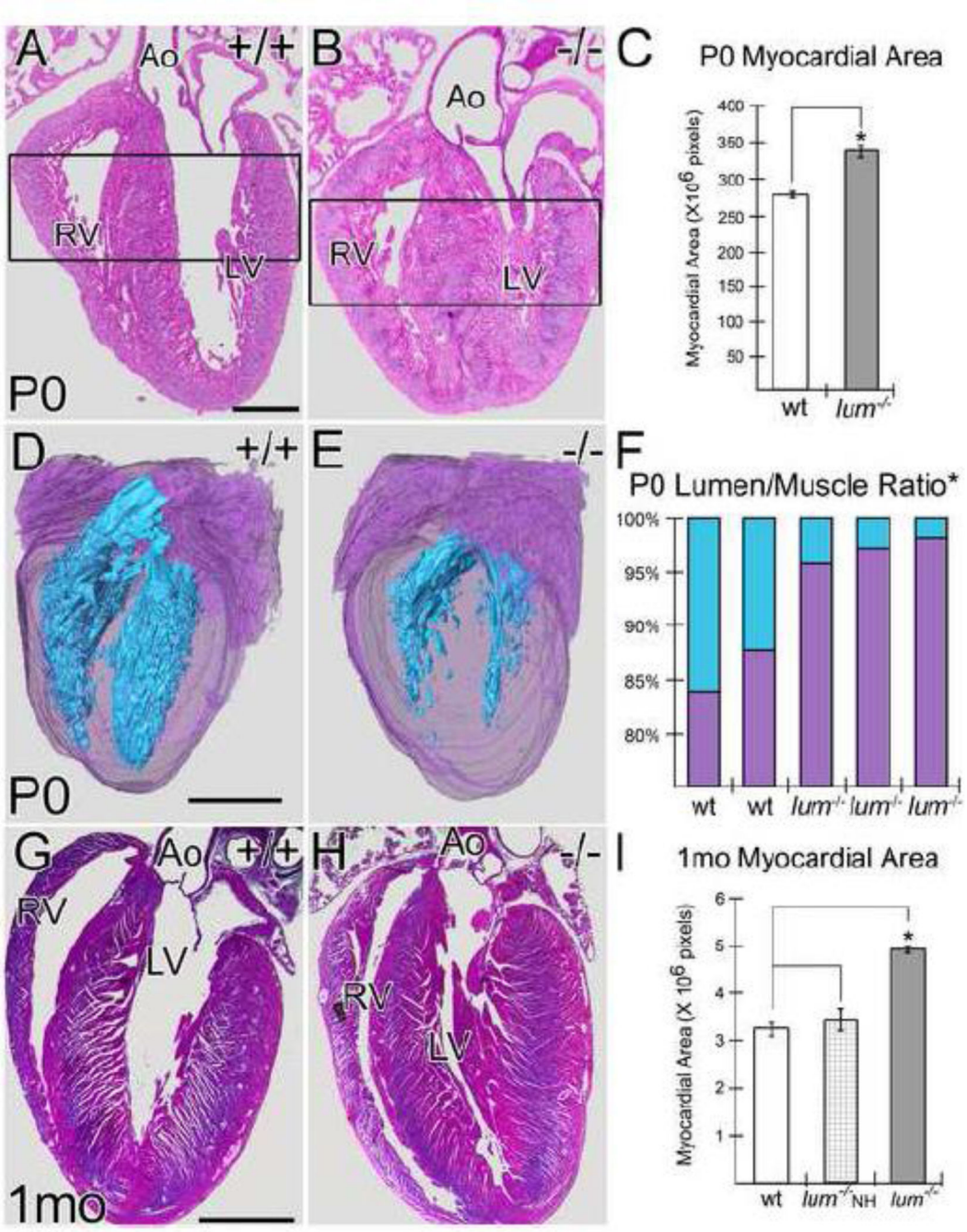


**Figure 2. Lumican deficient mice exhibited a significant increase in myocardial area and concomitant reduction in ventricular lumen size at Postnatal day 0 and one month**

Histological sections from WT (A) and *lum*$^{-/-}$ (B) P0 hearts with corresponding graph showing the average ventricular area (in pixels) of WT (n=4) and *lum*$^{-/-}$ (n=4) (C). Open rectangles (A, B) denotes area measured using Amira™. Three-dimensional reconstructions of WT (D) and *lum*$^{-/-}$ (E) P0 whole hearts (purple-myocardium; cyan-lumen). Graph in F shows percentage of muscle (purple) versus lumen (cyan) in two WT and three *lum*$^{-/-}$ reconstructions. Sections from 1 month (1 mo) juvenile WT (G) and *lum*$^{-/-}$ (H) hearts.

Graph in I denotes area in pixels of WT (open bar) with *lum*$^{-/-}$ hearts divided into non-hypertrophic (NH, cross-hatched) and hypertrophic (solid gray). Ao-aorta; RV-right ventricle; LV-left ventricle. *-statistical significance: C, $P < 2.0 \text{ X } 10^{-6}$ ; F, $P < 0.02$, % lumen area, $P < 0.02$, % muscle area; I, $P < 1.6 \text{ X } 10^{-6}$ . Bars in the graphs of C and I denote standard deviation. Magnification bars: A= 500 μm, D= 600 μm, G= 2 mm applies to G.

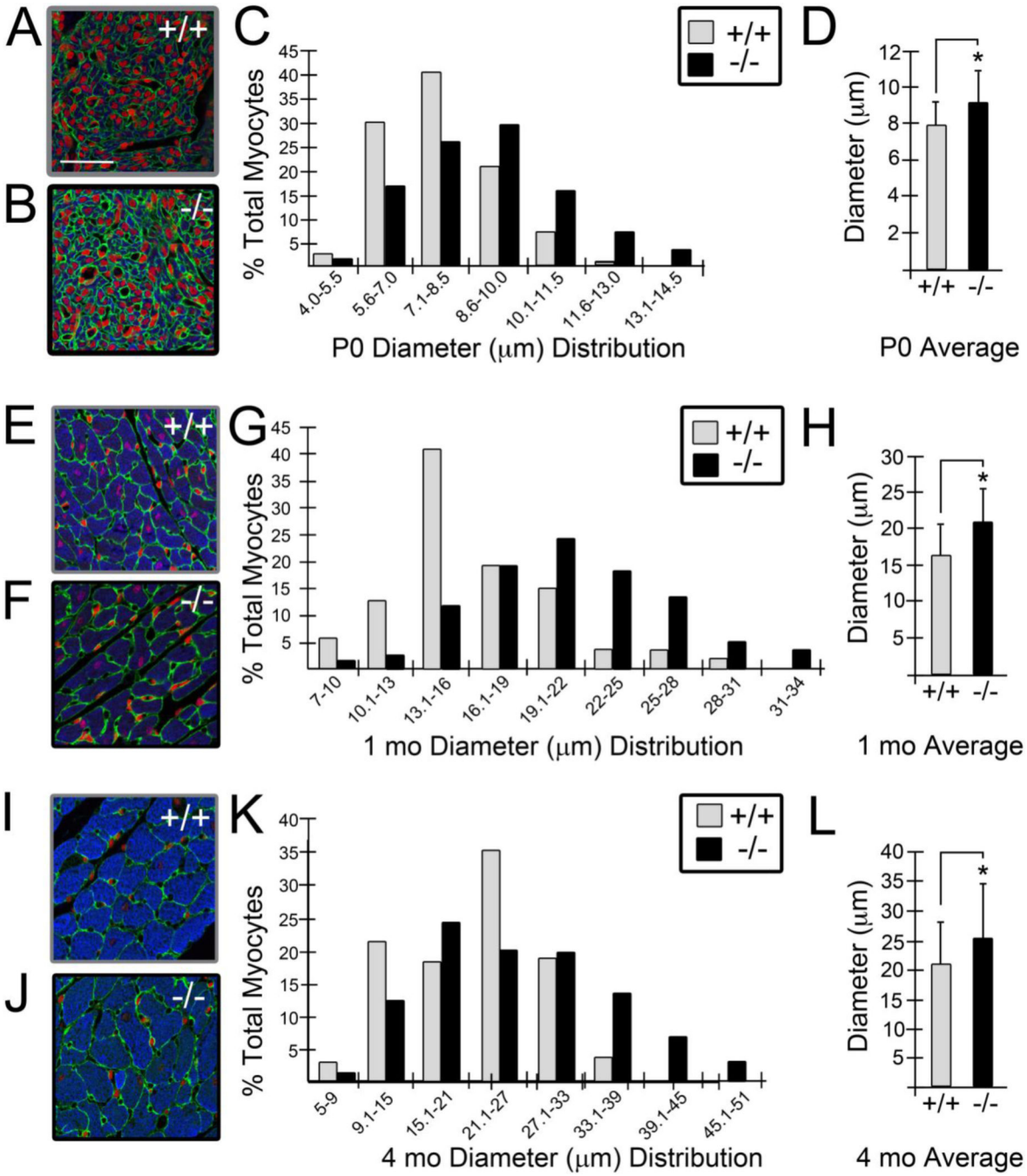


**Figure 3. Cardiomyocyte size was increased in lumican deficient mice**

The diameter of α -sarcomeric actin positive cardiomyocytes (blue, A, B, E, F, I, J) was measured in left ventricular (LV) tissue of *lum*$^{-/-}$ and WT littermate hearts at postnatal day 0 (P0, A–D; n=4 WT, n=4 *lum*$^{-/-}$), 1 month (1 mo, E-H; n=5 WT, n=8 *lum*$^{-/-}$) and adult (4 mo, I-L; n=3 WT, n=3 *lum*$^{-/-}$). The graphs in C, G, and K show the percentage of total cardiomyocytes (Y-axis) that fall into the size (μm) range of diameter groups designated on the X-axis. The average size of the cardiomyocytes in the LV of *lum*$^{-/-}$ was significantly larger than WT at P0 (D), 1 mo (H) and 4 mo (L). Error bars in D, H, L, show standard

deviation of cardiomyocyte diameters. * -denotes statistical significance: D, $P < 1.1 \text{ X } 10^{-8}$ ; H, $P < 2.3 \text{ X } 10^{-5}$ ; L, $P < 9.4 \text{ X } 10^{-6}$ . Grey bars denote WT and black bars designate $lum^{-/-}$ measurements. Green-A, B, E, F, I and J, shows laminin immunolocalization, red propidium iodide, and blue-α sarcomeric actin. Magnification bars: A = 50 μm and applies to B, E, F, I and J.

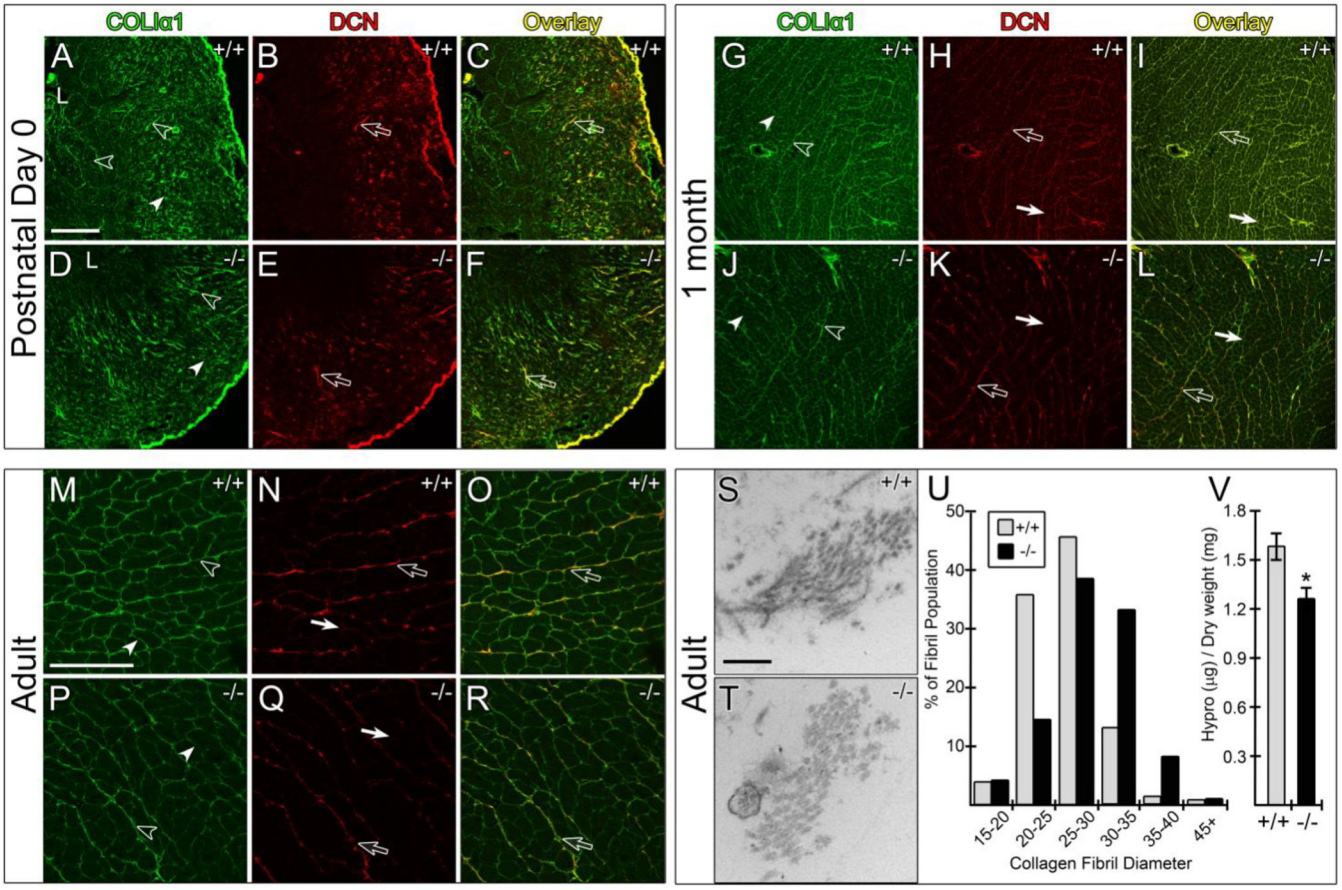


**Figure 4. Collagen 1 and DCN immunolocalization and electron microscopy reveal differences in 1 month and adult LUM deficient hearts**

Histological sections from WT and *lum*$^{-/-}$ LV at P0 (A–F), 1 mo (G–L) and adult (4 mo, M–R) were used for immunolocalization (IHC) of collagenα1(I) (green, A, D, G, J, M, P) and DCN (red, B, E, H, K, N, Q) with overlay in panels C, F, I, L, O and R appearing as yellow/yellowish-green. Solid arrowheads denote pericellular IHC of COLIα1 (A, D, G, J, M, P). Open arrowheads indicate perimysial, (sheath), collagenα1(I) IHC (A, D, G, J, M, P). Solid arrows (H, K, I, L, N, Q) show pericellular staining of DCN. Open arrows depict perimysial, staining of DCN (H, I, K, L, N, Q). +/+; WT samples, −/− : *lum*$^{-/-}$ . N= 4 each minimum of *lum*$^{-/-}$ and wild type littermate comparisons for *lum*$^{-/-}$ and DCN. L- lumen (A, D). Collagen fibril diameter was measured in adult hearts from WT (S) and *lum*$^{-/-}$ (T) and shown in the graph in U (grey bars denote WT and black bars designate *lum*$^{-/-}$). Total insoluble content as measured by hydroxyproline (Hypro) (V), * denotes $P < 2.34 \text{ X } 10^{-33}$ . Magnification bars: A=200 μm, applies to B–F and G–L; M=50 μm applies to N–R; S=200 nm applies to T.

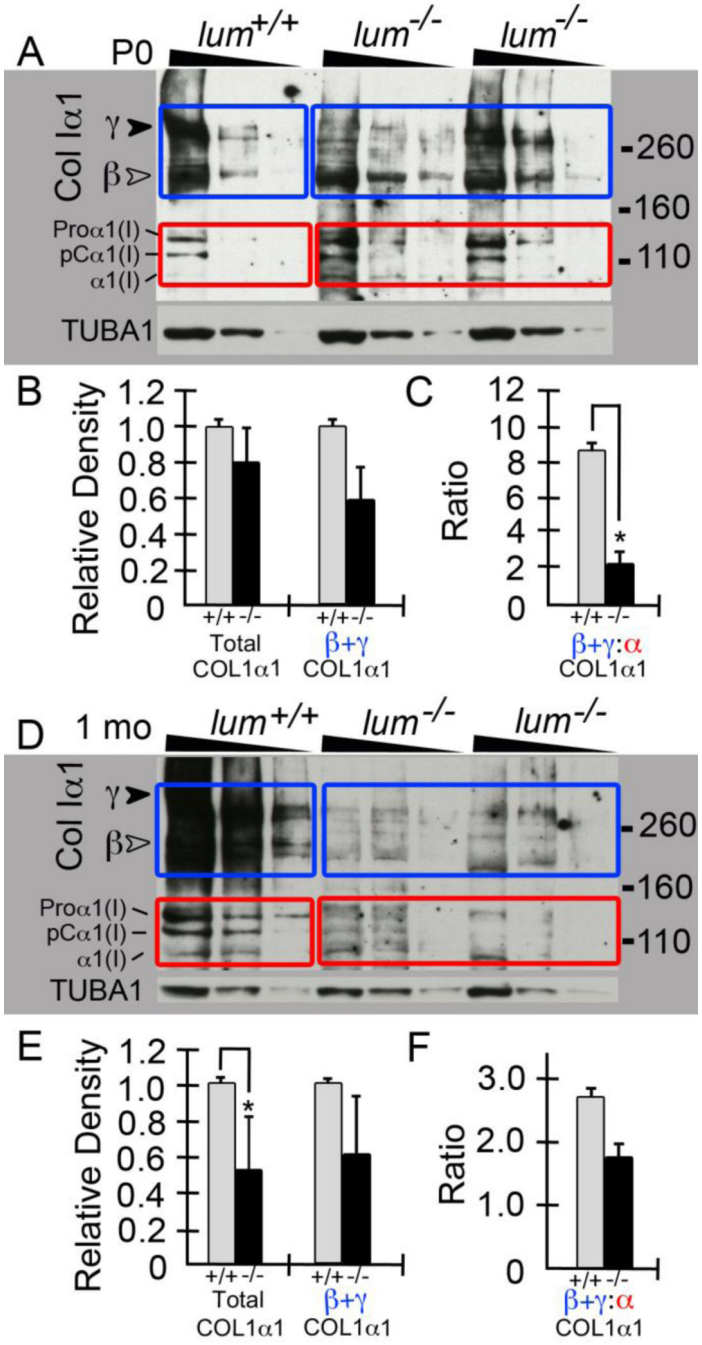


**Figure 5. Soluble Collagen 1 levels are reduced in heart extracts from lumican deficient mice at P0 and 1 month**

Gradient reducing gels (3–8%) using heart extracts from WT and *lum*$^{-/-}$ mice were probed for collagenα1(I). Triangles above lanes denote the sample loading at 50, 25, 12.5 μg total protein. Extracts from one WT and two *lum*$^{-/-}$ littermates are shown for P0 (A) and 1 mo (D). Blue boxes denote the β and γ collagenα1(I) bands in A and D. Red boxes highlight the α forms of collagenα1(I) (A, D). Graphs in B and C are densitometry quantification of all P0 (n=2 WT; n=3 lum$^{-/-}$) hearts comparing total collagenα1(I), the β and γ forms (B) and the

ratio of β and γ: α (C). Graphs in E and F show quantification of 1 mo hearts (n=2 WT, n=2 *lum*$^{-/-}$) comparing total collagenα1(I), the β and γ forms (E) and the ratio of β and γ: α (F). P0: * -denotes *P* <0.02; 1 mo * -denotes *P* <0.006. TUBA1: α-tubulin, loading control. Relative Density (Y-axis) based on Image J units.

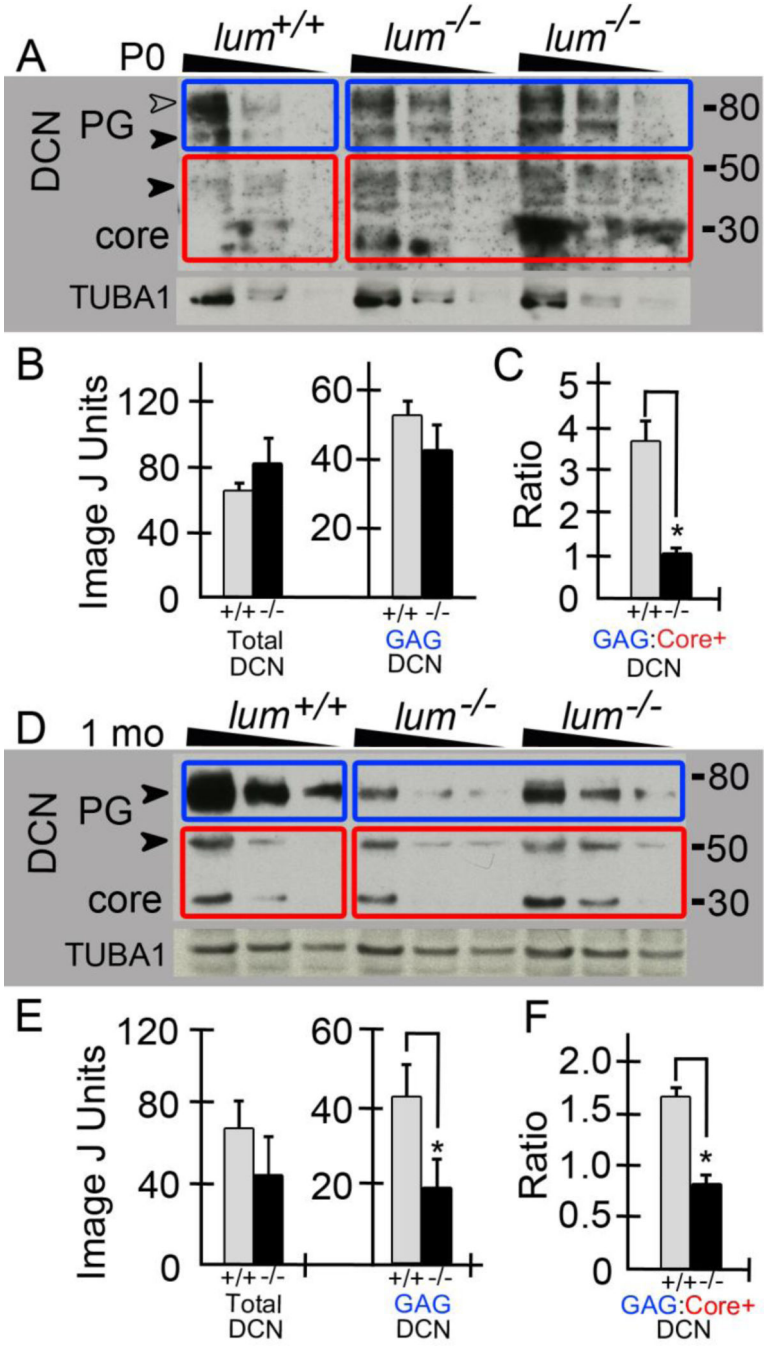


**Figure 6. The glycosaminoglycan containing forms of DCN are reduced in lumican deficient hearts at P0 and 1 month**

Heart extracts from WT and *lum*$^{-/-}$ deficient hearts at P0 (A; n=2 WT, n= 3 *lum*$^{-/-}$) and 1 mo (D; n=2 WT, n= 3 *lum*$^{-/-}$) were run on reducing gels (4–12%), blotted and probed for DCN. Triangles above lanes denote the triple loading at 50, 25 and 12.5μg total protein. Extracts from one WT and two different *lum*$^{-/-}$ from the same litter are shown for P0 (A) and 1 mo (D). The P0 hearts contained two GAG-containing forms of DCN around 95kD (A, open arrowhead, blue boxes) and 75kD (A, closed arrowhead). Red boxes bound the 50kD bands and core DCN at 30kD (A, D). Blue boxes in D denote GAG-containing form

of DCN at 1 mo. Graphs (B, C, E, F show densitometry values of all P0 DCN bands and reveal a significant difference in the GAG containing forms of DCN relative to core band at P0 (B, C) and 1 month (E, F). C * denotes P < 0.02, E * denotes $P < 0.04$, F * denotes $P < 0.04$. PG-proteoglycan. TUBA1: α-tubulin used for normalization.

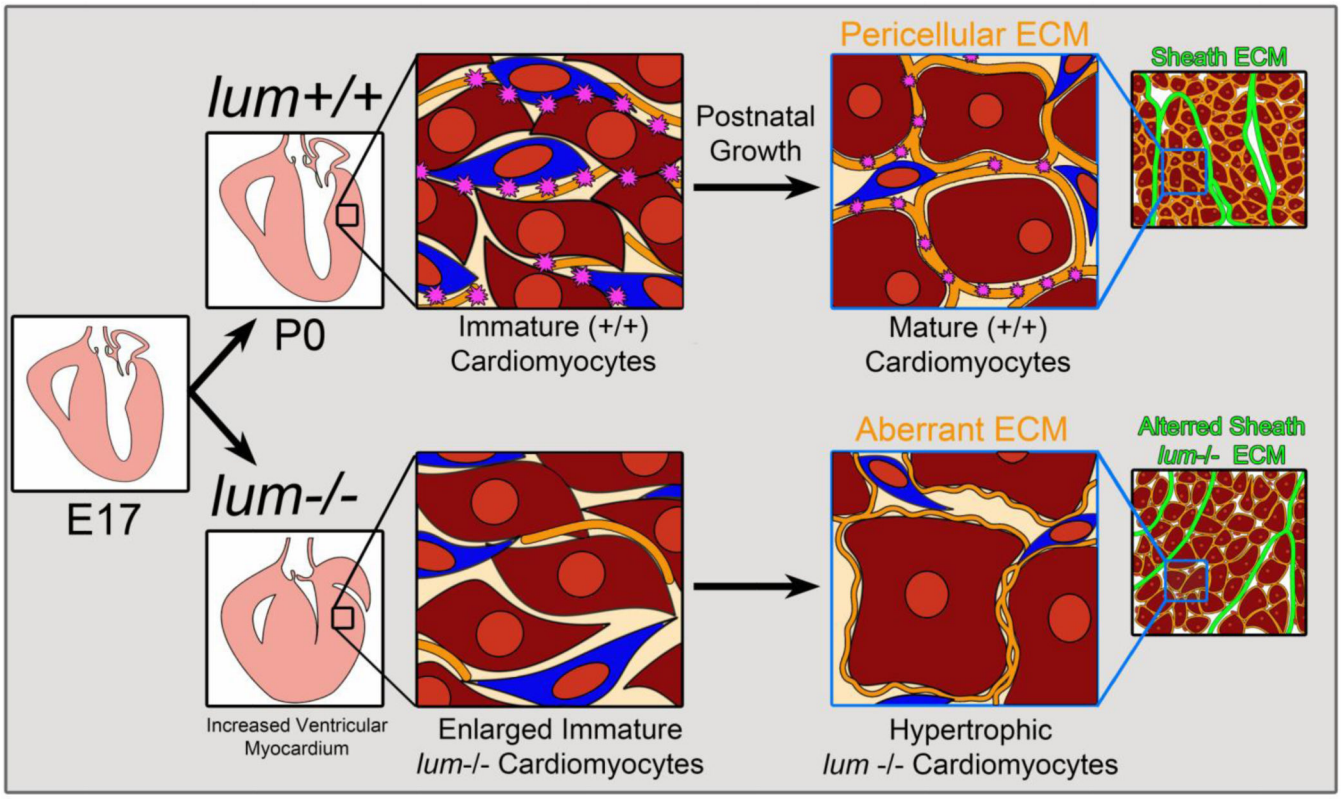


**Figure 7. Summary and working model of lumican deficiency in the murine heart**

There were no notable morphological differences in *lum*$^{-/-}$ hearts prior to birth (E17.5). After birth (P0) *lum*$^{-/-}$ hearts exhibited increased myocardial area due to enlarged immature (stellate-shaped) cardiomyocytes. As *lum*$^{-/-}$ cardiomyocytes matured the pericellular ECM was altered due in part to differences in collagenα1(I) and DCN. Considering these components also contribute to the sheath ECM we anticipate the perimysial ECM is also altered in the *lum*$^{-/-}$ deficient hearts.

Key: - pericellular cardiomyocyte ECM; -lumican; - fibroblast; -immature cardiomyocyte; -mature cardiomyocyte. -sheath ECM.